Journal of Cluster Science, Vol. 17, No. 2, June 2006 (© 2006)
DOI: 10.1007/s10876-006-0053-1

Inducing Molecular Growth in an $\{Mo_{57}Fe_6\}$-type Nanocluster: Synthesis, Structure, and Properties of $\{Mo_{57}(Mo)_2Fe^{III}_6\}$*

John Fielden,[1] Yurii L. Malaestean,[1] Arkady Ellern,[2] Ricardo García-Serres,[3] Leroy Cronin,[4] and Paul Kögerler[1,5]

Received January 23, 2006; published online March 10, 2006

The reaction of the polyoxomolybdate anion $[Mo^{VI}_{32}(MoNO)_4O_{108}(H_2O)_{16}]^{12-} = \{Mo_{36}(NO)_4\}$ with Fe^{II} salts and hydrazine sulfate yields the cluster anion $[Mo^{V/VI}_{51}(Mo^{VI}O)_2Fe^{III}_6(MoNO)_6O_{176}(OH)_3(H_2O)_{22}]^{15-}$ (**1a**), isolated as its corresponding ammonium salt $(NH_4)_{15}\mathbf{1a}\cdot 36H_2O$ (**1**) (space group $P6_3/mmc$, $a = b = 23.607(5)$ Å, $c = 26.767(6)$ Å, 4076 unique reflections, 293 parameters). Despite the absence of oxygen and the reducing conditions the product comprises only Fe^{III} centers as determined by a combination of spectroscopic, magnetic and crystallographic analysis. Reduction of peripheral Mo centers causes the aggregation of two additional $[Mo^{VI}O]^{4+}$ groups onto the archetypal $\{Mo_{57}M_6\}$ structure. The single-crystal X-ray determined structure of **1** is reported.

KEY WORDS: Polyoxometalates; polyoxomolybdates; iron(III); self-assembly; molecular magnetism; Mössbauer spectroscopy.

INTRODUCTION

The self-assembly of nanometer-sized polyoxomolybdate cluster structures is a focal point of current research due to their relevance in various fields of

*Dedicated to Professor Michael T. Pope.

Electronic Supplementary Material Supplementary material is available for this article at http://www.dx.doi.org/10.1007/s10876-006-0053-1 and is accessible for authorized users.

[1]Ames Laboratory, Iowa State University, Ames, IA 50011, USA.
[2]Department of Chemistry, Iowa State University, Ames, IA 50011, USA.
[3]Department of Physics, Emory University, Atlanta, GA 30322, USA.
[4]Department of Chemistry, University of Glasgow, Glasgow, G12 8QQ, UK.
[5]To whom correspondence should be addressed. E-mail: kogerler@ameslab.gov

molecular materials sciences, for instance catalysis, molecular magnetism, or molecular electronics [1]. While the exact mechanisms that underpin the formation processes of these molecules are not yet determined, nearly all nanosized polyoxomolybdate cluster structures can be formally deconstructed into sets of 'building blocks' [2, 3], i.e. transferable fragments. Synthetic approaches thus aim to combine or functionalize these building blocks and to expand the combinatorial building block library by generating novel types of linkable fragments [4]. A number of archetypal polyoxomolybdate structures, e.g. those of the molybdenum blue type [4], comprise the nearly planar $\{Mo_8\}$ building block, consisting of a pentagonal MoO_7 bipyramid with five MoO_6 octahedra fused to its equatorial edges and two additional, 1,3-positioned MoO_6 octahedra (Mo′) sharing corners with the central $\{(Mo)Mo_5\}$ fragment. Two such $\{Mo_8\}$ groups in turn are found fused into a C_s-symmetric, corrugated $\{Mo_{17}\}$-type building block [4]. While the two $\{Mo_8\}$ units here share four edges, an additional Mo center coordinates to the center of the resulting angled (by approx. 110°) $\{Mo_8\}_2$ structure. In this configuration the $\{Mo_{17}\}$ building block is for example observed in the isopolyoxomolybdate $[Mo^{VI}_{36}O_{112}(H_2O)_{16}]^{8-} = \{Mo_{36}\}$ [5] in which two $\{Mo_{17}\}$ building blocks are interlinked by two $[MoO_2]^{2+}$ groups. Both the $\{Mo_8\}$ and the $\{Mo_{17}\}$ building blocks can be modified using the nitrosylating agent hydroxylamine, resulting in the replacement of the apical vector $[MoO]^{4+}$ central to the pentagonal MoO_7 bipyramid by a $[MoNO]^{3+}$ group, thereby increasing the negative charge and the nucleophilicity of the cluster fragment. The corresponding $\{Mo_{36}(NO)_4\}$ derivative, $[Mo^{VI}_{32}(MoNO)_4O_{108}(H_2O)_{16}]^{12-}$ (**4a**) [6], displays an interesting reactivity toward electrophiles, e.g. divalent transition metal cations such as Fe^{2+} or VO^{2+} and forms cluster structures of the donut-shaped, D_{3h}-symmetric $\{Mo_{57}M_6\}$ type (Fig. 1).

The cluster anions $[Mo^{VI}_{51}(V^{IV}O(H_2O))_6(MoNO)_6O_{174}(OH)_3(H_2O)_{12}]^{21-}$ (**2a**), isolated as $(NH_4)_{21}$**2a**$\cdot 65\ H_2O$ (**2**) [6, 7] and $[Mo^{VI}_{51}(Fe^{III}(H_2O)_2)_6(MoNO)_6O_{174}(OH)_3(H_2O)_{12}]^{15-}$ (**3a**), isolated as $(NH_4)_{15}$**3a**$\cdot 73\ H_2O$ (**3**) [7, 8] are examples of this structure type. Here, three $\{Mo_{17}(NO)_2\}$ building blocks are arranged around a C_3 axis and interlinked via three $\{Mo^V_2\} = [O_3Mo^V(\mu_2\text{-}OH)(\mu_2\text{-}OH_2)_2Mo^VO_3]^{2-}$ groups and six octahedrally coordinated transition metal cations *trans*-$[ML_2]^{n+}$ (L = O, OH_2) that occupy the vertices of a trigonal prism with intra-triangle M–M distances of approx. 6.5 Å and inter-triangle distances of approx. 9.6 Å (Fig. 2).

The $\{Mo^V_2\}$ groups consist of two face-sharing MoO_6 octahedra that share three corners with each of the two $\{Mo_{17}\}$ groups they interlink. The Mo···Mo distance ranges from 3.31 to 3.35 Å in these structures, but Extended Hückel Molecular Orbital and PM3 calculations indicate that the Mo–Mo interaction in this particular type of $\{Mo^V_2\}$ group has antibonding

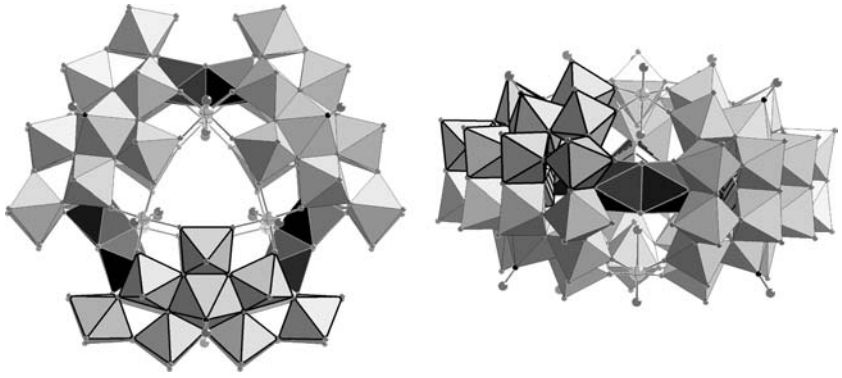

Fig. 1. Polyhedral representation of the $\{Mo_{57}M_6\}$ structure type seen along the C_3 axis (left) and along a C_2 axis (right) emphasizing one $\{Mo_8\}$ group (light gray, dark outline). The three $\{Mo^{V}{}_2\}$ groups are shown in dark gray, and the six transition metal positions in a ball-and-stick representation (M positions crossed).

character. The degree of protonation of the bridging oxo groups has been established through Bond Valence Sum calculations and has recently been confirmed by single-crystal neutron diffraction studies [9]. The μ_2-hydroxo ligand is situated in the C_s plane of the molecule, while the two μ_2-water ligands are positioned out-of-plane (above and below the C_s plane).

A number of different spin centers such as V^{IV} ($s = 1/2$), Cu^{II} ($s = 1/2$), $Fe^{II/III}$ ($s = 2,\ 5/2$), and mixtures thereof, can be embedded in the rigid, otherwise diamagnetic polyoxomolybdate framework, allowing 'tuning' of the magnetic properties based on the composition of the M_6 substructure. Strong and weak antiferromagnetic [7, 10], ferrimagnetic [10] and weak

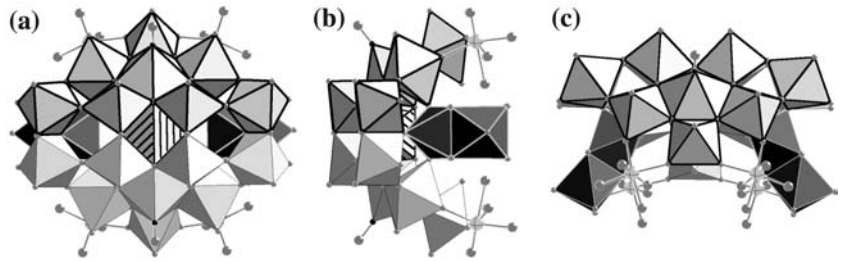

Fig. 2. A representative section of a $\{Mo_{57}M_6\}$ structure illustrating the corner-sharing connections between the building blocks: Polyhedral plot of one $\{Mo_{17}\}$ building block (one $\{Mo_8\}$ half highlighted by dark edges, with two adjoined $\{Mo^{V}_2\}$ groups (dark gray) and four coordinated {M} groups (ball-and-stick) in three perpendicular views: (a) along C_2, (b) perpendicular to C_2, (c) approx. along C_3. The MoO_6 octahedra central to the $\{Mo_{17}\}$ groups are shown hatched.

ferromagnetic [11] nearest-neighbor magnetic exchange coupling has been realized in such $\{Mo_{57}M_6\}$ systems thus far.

Moreover, if the synthesis of $\{Mo_{57}V_6\}$ **2a** is carried out in the presence of a strong reducing agent, the $\{Mo_{17}\}$ groups are partially reduced so that Mo positions surrounding the gaps between the $\{Mo_{17}\}$ groups are reduced to Mo^{V}, rendering these pockets more nucleophilic. Consequently, up to six electrophilic $[Mo^{VI}O]^{4+}$ groups are found to occupy these sites, binding to two terminal oxo positions of two neighboring, reduced Mo centers and one former μ_2-OH_2 group of the adjacent $\{Mo_2^{V}\}$group that becomes completely deprotonated. In this configuration the added Mo centers assume a tetrahedral coordination environment. As the stepwise uptake of each $[MoO]^{4+}$ group coincides with an addition of two Mo(4d) electrons and the loss of two protons, the cluster net charge remains unchanged and cluster species $[Mo_{51}(VO(H_2O))_6(MoO)_n(MoNO)_6O_{173+n}(OH)_3(H_2O)_{12-n}]^{21-} = \{Mo_{57}Mo_nV_6\}$ **5a** ($n = 1$–6) result [12, 13]. Interestingly, this type of molecular growth, confined to the pre-defined pockets of the host cluster structure, appears to be reversible, whereby the $[MoO]^{4+}$ groups are released upon oxidation of the $\{Mo_{57}Mo_nV_6\}$ system [12]. The study of these types of molecular aggregation/disintegration are of special value in polyoxomolybdate chemistry as they provide insight into the mechanisms underlying the formation of larger cluster systems.

Here we report that this type of molecular growth is also observed for $\{Mo_{57}Fe_6\}$-type host structures under reducing conditions. We describe the isolation of the product $(NH_4)_{15}[Mo_{51}^{V/VI}(Mo^{VI}O)_2Fe_6^{III}(MoNO)_6O_{176}(OH)_3(H_2O)_{22}] \cdot 36\ H_2O$ **1** which has been characterized by single-crystal X-ray diffraction (including Bond Valence Sum calculations), IR spectroscopy, elemental analysis, thermogravimetry and differential scanning calorimetry (DSC), potentiometric titrations, magnetic measurements and Mössbauer spectroscopy.

EXPERIMENTAL SECTION

Materials, Methods and Instrumentation

$(NH_4)_{12}[Mo_{36}(NO)_4O_{108}(H_2O)_{16}] \cdot 33H_2O$ (**4**) was synthesized according to literature methods [12]. Nitrogen-saturated distilled water was prepared by redistilling water under nitrogen (70 to 90 mbar) on a rotary evaporator, refilling the apparatus to atmospheric pressure with nitrogen, and further purging with bubbling nitrogen before storage. All other reagents were obtained commercially as ACS reagent grade and used as received. Infra-red spectra were measured with a Bruker Tensor 27, UV/VIS/NIR spectra with a Shimadzu UV-1650PC spectrophotometer, redox

titrations performed with a Mettler Toledo DL50 titrator, thermogravimetric and calorimetric analyses (reproduced for three different sample batches) on a Perkin Elmer TGA 7 and DSC 7, and elemental analysis on a Perkin Elmer 2400 CHNS Analyzer. Single-crystal X-ray diffraction data were collected on a Bruker CCD-1000 diffractometer with MoK_α radiation and a graphite monochromator. Magnetic measurements were performed in the range of 2–290 K with a Quantum Design MPMS-5 SQUID magnetometer for a range of fields from 0.1 to 5.0 T. Susceptibility data were corrected for diamagnetic and temperature-independent paramagnetic (TIP) contributions that were calculated from tabulated values and from measurements on **4** ($\chi_{dia/TIP}(\mathbf{1}) = -1.23 \times 10^{-3}$ emu mol^{-1}). Mössbauer spectra were recorded on a weak-field Mössbauer spectrometer operated in a constant acceleration mode in a transmission geometry. The zero velocity of the Mössbauer spectra refers to the centroid of the room temperature spectrum of a metallic iron foil.

Synthesis of $(NH_4)_{15}[H_3Mo_{59}Fe_6(NO)_6O_{181}(H_2O)_{22}] \cdot 36H_2O(\mathbf{1})$

$(NH_4)_{12}[Mo_{36}(NO)_4O_{108}(H_2O)_{16}] \cdot 33\ H_2O$ (**4**, 4.00 g, 0.62 mmol) and $(NH_4)_2SO_4FeSO_4 \cdot 6\ H_2O$ (8.82 g, 22.5 mmol) were placed in a 100 mL Schlenk flask which was then evacuated and refilled with argon. Addition of nitrogen-saturated distilled water (40 mL) followed by hydrazine sulfate ($N_2H_4 \cdot H_2SO_4$; 0.08 g, 0.62 mmol) and stirring at 70°C for 18 h under an argon atmosphere resulted in a deep blue–black solution which was quickly filtered into a 125 mL Erlenmeyer flask and purged of air by bubbling argon. The flask was sealed and allowed to cool to room temperature resulting in isolation of small dark blue–black crystals of $(NH_4)_{15}[H_3Mo_{59}Fe_6(NO)_6O_{181}(H_2O)_{22}] \cdot 36\ H_2O$ (0.944 g, 0.091 mmol, 24 % relative to Mo) in 24–48 h. Analysis for $H_{179}Fe_6Mo_{59}N_{21}O_{245}$ Calcd. (found) %: H 1.74 (1.73), N 2.83 (2.82). FTIR (KBr disc), cm^{-1}: 3426m, 3133s, 1602s, 1400s, 947w, 879vs, 821w, 768m, 665w, 620m, 591m, 545m, 421w. UV/VIS (solution): $\lambda_{max} = 766$ nm ($\varepsilon = 2560$ L mol^{-1} cm^{-1}).

Potentiometric titrations

Measurements were performed on five individual sample batches using a Mettler Toledo DL50 titrator. Each time the compound $(NH_4)_{15}[H_3Mo_{59}Fe_6(NO)_6O_{181}(H_2O)_{22}] \cdot 36\ H_2O$ **1** (typically approx. 0.20 g, 0.019 mmol) was fully oxidized by gentle heating with $(NH_4)_2Ce(NO_3)_6$ (typically approx. 0.36 g, 0.66 mmol) in 0.5 M aqueous H_2SO_4 (50 mL). The excess amount of Ce^{IV} was then back-titrated with 0.1 N $NaNO_2$. Titrations of several batches of **4** under such conditions resulted in 14.0 ($\pm$0.2) electrons per cluster anion.

Single-Crystal Structure Determination

A suitable single crystal of $(NH_4)_{15}[H_3Mo_{59}Fe_6(NO)_6O_{181}(H_2O)_{22}]\cdot 36\ H_2O$ **1** was mounted on the end of a thin glass fiber using epoxy glue, under ambient conditions. X-ray diffraction intensity data were measured at 293 K on a Bruker CCD-1000 diffractometer ($\lambda(MoK_\alpha) = 0.7107$ Å). Measurements at lower temperatures were obstructed by thermal stress-induced cracking of the crystals. The initial unit cell was determined from three sets of ω scans at different starting angles, with the obtained reflections being successfully indexed by an automated indexing routine built in the SMART program. The final cell constants were calculated from a set of strong reflections from the actual data collection. Structure solution and refinement was carried out with SHELXTL software [14], and also SHELXL97 via WinGX [15]. Corrections for incident and diffracted beam absorption effects was based on fitting a function to the empirical transmission surface as sampled by multiple equivalent measurements [16] using SADABS software [14]. The compound crystallizes in the space group $P6_3/mmc$ as determined by systematic absences in the intensity data, intensity statistics and the successful solution and refinement of the structure. The structure was solved by a combination of direct methods and difference Fourier syntheses and refined against F^2 by the full-matrix least-squares technique. Crystal data, data collection parameters and refinement statistics are in Table I.

RESULTS AND DISCUSSION

The reaction of the cluster anion $\{Mo_{36}(NO)_4\}$ **4a** with a small amount of the reducing agent hydrazine sulfate and a large excess of Fe^{II} (molar ratios **4a**: $N_2H_6SO_4$: $Fe^{II} = 1{:}36{:}1$) in aqueous solution in the absence of oxygen yields the cluster anion $[Mo^{V}_4Mo^{VI}_{47}(Mo^{VI}O)_2Fe^{III}_6(MoNO)_6O_{176}(OH)_3(H_2O)_{22}]^{15-}$ **1a**. The cluster structure derived from single-crystal X-ray diffraction (Table I) consists of the critical constituents of the $\{Mo_{57}M_6\}$ structure type: three $\{Mo_{17}\}$ and three $\{Mo^{V}_2\}$ building blocks and six transition metal cations, here *trans*-$[Fe(H_2O)_2]^{3+}$ groups. **1a** is derived from the structure of the aforementioned cluster anion $[Mo^{VI}_{51}(Fe^{III}(H_2O)_2)_6(MoNO)_6O_{174}(OH)_3\ (H_2O)_{12}]^{15-}$ **3a** but features additional $[MoO]^{4+}$ groups (Mo8-O23: 1.767 Å) (Fig. 3a). These are disordered over the six central sites in the gaps between the three $\{Mo_{17}\}$ building blocks, binding to a trigonal O_3 motif of two terminal oxo positions (O24, belonging to the Mo′ positions (Mo6) of the $\{Mo_8\}$ motifs) and to one out-of-plane μ_2-O position (O22) of the $\{Mo^{V}_2\}$ group interlinking the respective $\{Mo_{17}\}$ fragments (Fig. 3). In coordinating to this nearly equilateral O_3

Table I. Crystallographic Data for $(NH_4)_{15}[H_3Mo_{59}Fe_6(NO)_6O_{181}(H_2O)_{22}] \cdot 36\ H_2O$

Empirical formula	$H_{179}\ Fe_6\ Mo_{59}\ N_{21}O_{245}$
Formula weight (g/mol)	10390.20
Space group	$P6_3/mmc$
a (Å)	23.607(5)
b (Å)	23.607(5)
c (Å)	26.767(6)
α (°)	90°
β (°)	90°
γ(°)	120°
V (Å^3)	12,919(5) Å^3
Z	2
Temperature (K)	293(2) K
ρ_{calc} (g cm^{-3})	2.671
μ (mm^{-1})	3.196
No. observations (unique)	93,138 (4076)
No. parameters	293
Residuals: $R1$; $wR2$*	0.0592; 0.1915

* $R1 = \Sigma||F_o| - |Fc||/\Sigma|Fo|.wR2 = \{\Sigma[w(F_o^2 - F_c^2)^2]/\Sigma[w(F_o^2)^2]\}^{1/2}$.

triangle (O22···O24: 2.994 Å, O24···O24′: 3.083 Å) the Mo center assumes a tetrahedral coordination mode in which it is slightly shifted towards O22 and O23 (Fig. 3b, cf. Table II).

The insertion of the $[MoO]^{4+}$ groups induces a slight widening of the 'cavities' between the Mo_{17} groups: While the Mo5···Mo5′ distance within the $\{Mo_2^V\}$ groups of 3.315 Å remains nearly identical compared to the corresponding distance of 3.317 Å in **3a**, the Mo6···Mo6′ distance increases to 6.432 Å (from 6.345 Å in **3a**). The occupancy factors for the Mo8 and O23 positions, summed up over all six sites, add up to approx. two.

Correspondingly, the Mo′ (Mo6) positions **1a** display reduced BVS values (5.8). Redox titrations, corrected for the oxidation of the six $[MoNO]^{3+}$ groups and the three $\{Mo^V{}_2\}$ groups in **1a**, indicate the presence of 4.9 (±1) Mo(4d) electrons, in accordance with the observation for $\{Mo_{57}Mo_nV_6\}$-type systems that the uptake of each $[MoO]^{4+}$ group coincides with a twofold reduction of the molybdenum framework. The intense dark-blue color (broad absorption maximum around 760 nm) exhibited by **1** points to the fact that the Mo(4d) electrons are at least partly delocalized over other Mo centers of the $\{Mo_{17}\}$ units.

Surprisingly, despite the reducing conditions applied in the reaction solution, all six Fe positions in **1a** are of oxidation state +III, as indicated by their BVS values (3.2), by the observed magnetic moment and by its Mössbauer spectrum (Fig. 4). Given the absence of external oxidizers such

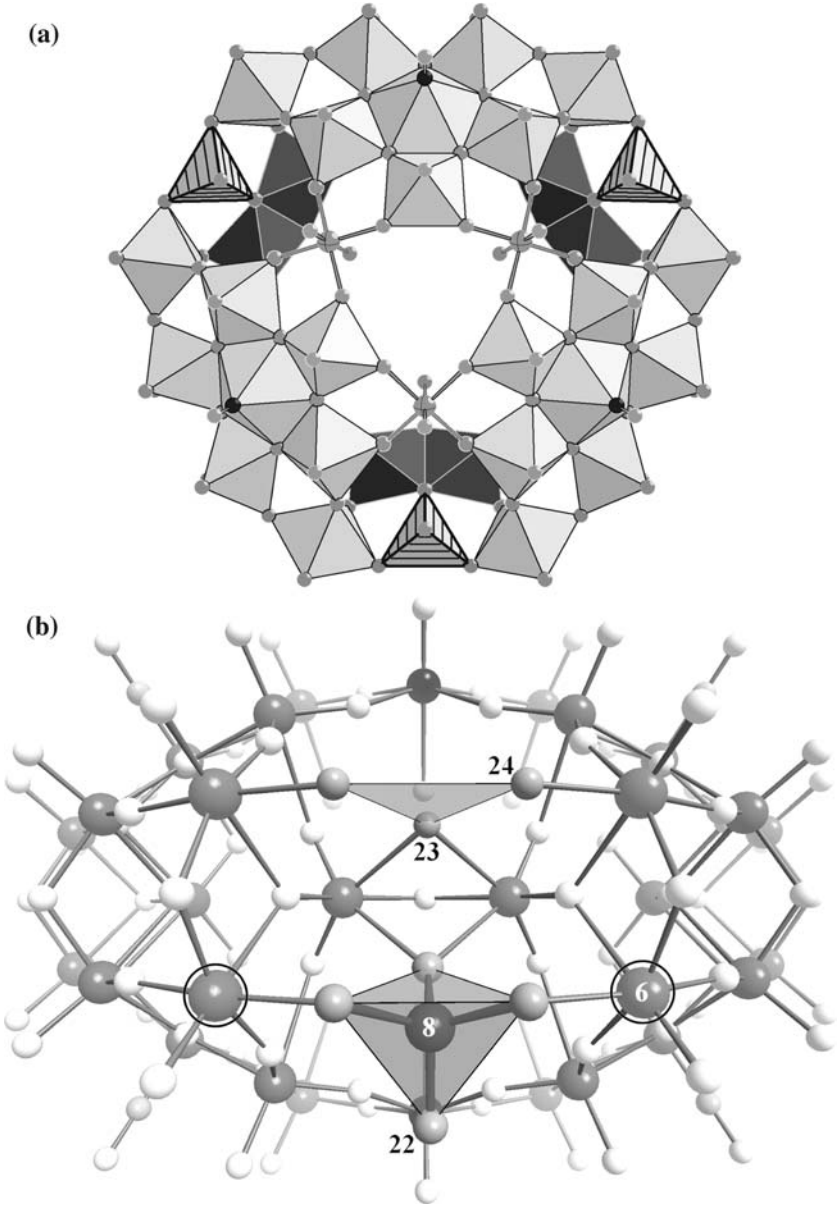

Fig. 3. (a) Polyhedral representation of the $\{Mo_{59}M_6\}$ cluster anion **1a** along C_3 axis emphasizing the underoccupied MoO_4 tetrahedra (hatched) that are added to the $\{Mo_{57}Fe_6\}$ host structure. (b) Ball-and-stick representation with selected atom numbers (along C_2) showing the trigonal O_3 binding motif (O23, O24, above) and the tetrahedral coordination mode of one $[MoO]^{4+}$ group (below). The bordering Mo′ centers (Mo6, encircled) are reduced, increasing the nucleophilicity of the 'cavities' between the $\{Mo_{17}\}$ groups.

Table II. Intramolecular Bond Distances and Angles for the External, 4-Coordinate Molybdenum Coordination Spheres in $(NH_4)_{15}[H_3Mo_{59}Fe_6(NO)_6O_{181}(H_2O)_{22}] \cdot 36H_2O$

Distances

Atom		Atom	Distance (Å)	Atom	Atom	Distance (Å)	
Mo(8)		O(23)	1.77(3)	Mo(8)	O(24)#1	1.879(12)	
Mo(8)		O(22)	1.79(2)	Mo(8)	O(24)	1.880(12)	
Angles							
Atom	Atom	Atom	Angle (deg)	Atom	Atom	Atom	Angle (deg)
O(23)	Mo(8)	O(22)	109.2(16)	O(23)	Mo(8)	O(24)	109.8(7)
O(23)	Mo(8)	O(24)#1	109.3(7)	O(22)	Mo(8)	O(24)	109.2(6)
O(22)	Mo(8)	O(24)#1	109.2(6)	O(24)#1	Mo(8)	O(24)	110.1(8)

as air/O_2 and the presence of a strong reducing reagent in the reaction solution, it appears that an initial reduction of polyoxomolybdate intermediates by Fe(II) is crucial and involves coordination of iron(II) centers that, after one-electron redox steps, remain coordinated to the emerging cluster fragment. Correspondingly, if the Fe(II) salt is replaced by a Fe(III) reagent in the reaction leading to **1** an amorphous iron polymolybdate immediately precipitates and the formation of any $\{Mo_{57}Fe_6\}$-type species is not observed. The low-field (0.1 and 1.0 T) magnetic susceptibility data, measured from 2 to 290 K, are virtually identical to the published results for $\{Mo_{57}Fe^{III}{}_6\}$ **3** [7], featuring weak antiferromagnetic intra-triangle and inter-triangle superexchange between the high-spin ($s = 5/2$) Fe^{III} centers. The Fe^{III} centers occupy a slightly distorted octahedral coordination environment (cf. Table III) that is characterized by two different Fe-OH_2 bond distances. The outward-oriented water ligand features a shorter Fe–O distance of 1.965 Å while the Fe–O bond distance to the *trans*-positioned water ligand (situated inside the cluster framework) is elongated to 2.208 Å (compared to 2.053 and 2.140 Å, respectively, for **3a** [8b]).

Furthermore, compared to the $\{Mo_{57}Fe_6\}$ cluster anion **3a** of identical charge, **1a** crystallizes in a much closer packed structure with only 36 crystal water molecules per cluster anion, with the molar volume V/Z reduced from 6659.6 $Å^3$ (**3**, which also crystallizes in a hexagonal crystal system, space group $P6_3/mmc$ [8b]) to 6459.5 $Å^3$ (**1**). This number of crystal water molecules is confirmed by thermogravimetric analysis (TGA), DSC, and elemental analysis (see supplementary data).

In summary, a $\{Mo_{57}(Mo)_2\ Fe^{III}_6\}$ cluster **1a** has been identified that resembles all features of the type of molecular growth observed for $\{Mo_{57}V_6\}$-type systems, now applied to a $\{Mo_{57}Fe_6\}$-type system. The

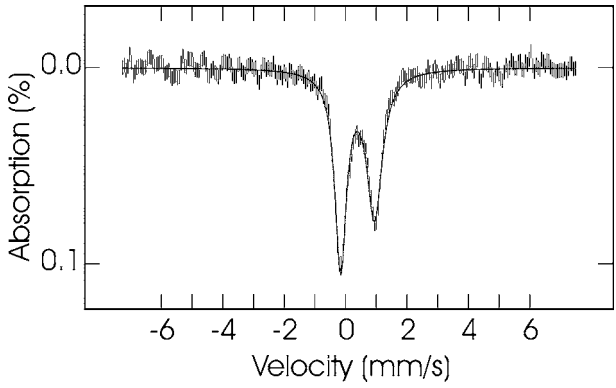

Fig. 4. Mössbauer spectrum of **1** recorded at 298 K in a 500 Gauss magnetic field applied parallel to the γ-beam. The spectrum is fitted with an asymmetric quadrupole doublet of Lorentzians, yielding the parameters $\delta = 0.39$ mm/s, $\Delta E_Q = 1.10$ mm/s, $\Gamma_L = 0.45$ mm/s, and $\Gamma_R = 0.62$ mm/s. These parameters are indicative of high-spin Fe(III) in a slightly distorted octahedral coordination. No Fe(II) is observed.

Table III. Intramolecular Bond Distances and Angles for the Iron Coordination Sphere of $(NH_4)_{15}[H_3Mo_{59}Fe_6(NO)_6O_{181}(H_2O)_{22}] \cdot 36H_2O$

Distances

Atom	Atom	Distance (Å)	Atom	Atom	Distance (Å)
Fe(1)	O(7)#1	1.940(9)	Fe(1)	O(8)#1	1.962(10)
Fe(1)	O(7)	1.940(9)	Fe(1)	O(8)	1.963(10)
Fe(1)	O(10)	1.965(14)	Fe(1)	O(12)	2.208(13)

Angles

Atom	Atom	Atom	Angle (deg)	Atom	Atom	Atom	Angle (deg)
O(7)#1	Fe(1)	O(7)	89.6(5)	O(10)	Fe(1)	O(8)	93.0(5)
O(7)#1	Fe(1)	O(10)	92.6(4)	O(8)#1	Fe(1)	O(8)	89.6(6)
O(7)	Fe(1)	O(10)	92.6(5)	O(7)#1	Fe(1)	O(12)	86.8(4)
O(7)#1	Fe(1)	O(8)#1	90.2(4)	O(7)	Fe(1)	O(12)	86.8(4)
O(7)	Fe(1)	O(8)#1	174.4(5)	O(10)	Fe(1)	O(12)	179.2(6)
O(10)	Fe(1)	O(8)#1	93.1(5)	O(8)#1	Fe(1)	O(12)	87.5(4)
O(7)#1	Fe(1)	O(8)	174.4(4)	O(8)	Fe(1)	O(12)	87.5(4)
O(7)	Fe(1)	O(8)	90.2(4)				

reducing conditions in the reaction solution of **1** cause a partial reduction of the polyoxomolybdate cluster framework, thereby increasing its nucleophilicity and its ability to attract and bind electrophiles, resulting (formally) in

the addition of two $[MoO]^{4+}$ groups to the $\{Mo_{57}Fe_6\}$ system **3a** that is reproduced as a substructure in **1a**. Future studies will explore the possibilities of extending this type of molecular growth to add additional electrophiles and to probe whether similar growth processes can be induced for similar $\{Mo_{57}M_6\}$-type (M = Cu, V/Fe) host systems.

SUPPLEMENTARY MATERIAL

IR and UV/VIS/NIR spectra and TGA and DSC curves; CIF tables for the crystal structure analysis of compound **1** may be obtained from the Fachinformationszentrum Karlsruhe, 76344 Eggenstein-Leopoldshafen, Germany (Fax: +49-7247-808-666; E-mail: crysdata@fiz-karlsruhe.de) on quoting the depository CSD no. 416051.

ACKNOWLEDGEMENTS

Ames Laboratory is operated for the U.S. Department of Energy by Iowa State University under Contract No. W-7405-Eng-82. Y.L.M. thanks MRDA/CRDF for a travel fellowship (award no. MTFP-04–03). We thank Professor B. H. Huynh for the ^{57}Fe Mössbauer data.

REFERENCES

1. C. L. Hill (1998). *Chem. Rev.* **98**, 1 (special issue on polyoxometalates).
2. A. Müller, P. Kögerler, and A. W. M. Dress (2001). *Coord. Chem. Rev.* **222**, 193.
3. A. Müller, P. Kögerler, and C. Kuhlmann (1999). *Chem. Commun.* 1347.
4. D.-L. Long, P. Kögerler, L. J. Farrugia, and L. Cronin (2003). *Angew. Chem. Int. Ed.* **42**, 4180; D.-L. Long, P. Kögerler, L. J. Farrugia, and L. Cronin (2005). *Dalton Trans.* 1372.
5. B. Krebs, S. Stiller, K. H. Tytko, and J. Mehmke (1991). *Eur. J. Solid Stat. Inorg. Chem.* **28**, 883.
6. A. Müller, E. Krickemeyer, S. Dillinger, H. Bögge, W. Plass, A. Proust, L. Dloczik, C. Menke, J. Meyer, and R. Rohlfing (1994). *Z. Anorg. Allg. Chem.* **620**, 599.
7. D. Gatteschi, R. Sessoli, W. Plass, A. Müller, E. Krickemeyer, J. Meyer, D. Sölter, and P. Adler (1996). *Inorg. Chem.* **35**, 1926.
8. (a) A. Müller, W. Plass, E. Krickemeyer, S. Dillinger, H. Bögge, A. Armatage, A. Proust, C. Beugholt, and U. Bergmann (1994). *Angew. Chem., Int. Ed. Engl.* **33**, 849; (b) A. Müller, H. Bögge, E. Krickemeyer, and S. Dillinger (1994). *Bull. Pol. Acad. Sci. Chem.* **42**, 291.
9. H. D. Lutz, R. Nagel, S. A. Mason, A. Müller, H. Bögge, and E. Krickemeyer (2002). *J. Solid State Chem.* **165**, 199.
10. A. Müller, W. Plass, E. Krickemeyer, R. Sessoli, D. Gatteschi, J. Meyer, H. Bögge, M. Kröckel, and A. X. Trautwein (1998). *Inorg. Chim. Acta* **271**, 9.
11. P. Kögerler and A. Müller (2003). *J. Appl. Phys.* **93**, 7101.
12. A. Müller, J. Meyer, E. Krickemeyer, C. Beugholt, H. Bögge, F. Peters, M. Schmidtmann, P. Kögerler, and M. J. Koop (1998). *Chem. Eur. J.* **4**, 1000.

13. A. Nicoara, A. Patrut, D. Margineanu, and A. Müller (2003). *Electrochem. Commun.* **5**, 511.
14. G. M. Sheldrick, *SHELXTL Version 5.1* (Bruker Analytical X-Ray Systems, Inc., Madison, WI, 1997).
15. L. J. Farrugia (1999). *J. Appl. Crystallogr.* **32**, 837.
16. R. H. Blessing (1995). *Acta Crystallogr* **A51**, 33.